J Nanopart Res (2011) 13:2909–2918
DOI 10.1007/s11051-010-0180-3

RESEARCH PAPER

Thermo- and pH-responsive hydrogel-coated gold nanoparticles prepared from rationally designed surface-confined initiators

Hye Hun Park · T. Randall Lee

Received: 11 February 2010 / Accepted: 8 December 2010 / Published online: 28 December 2010

Abstract Gold nanoparticles (~40 nm in diameter) were encapsulated by a hydrogel overlayer generated by the free radical polymerization of *N*-isopropylacrylamide-*co*-acrylic acid (NIPAM-co-AA), which was promoted by a specifically designed radical initiator covalently anchored to the surface of the gold core. The size and morphology of the shell/core nanoparticles were characterized by scanning electron microscopy and transmission electron microscopy. In addition, the optical properties of the nanoparticles were characterized by UV–Visible spectroscopy. Separately, the particle size was evaluated as a function of temperature and pH using dynamic light scattering. The shell/core hydrogel nanoparticles undergo reversible volume changes in water at a lower critical solution temperature (LCST) of ~34 °C as well as at pH values between 3 and 4. The unique composition and properties of these shell/core hydrogel nanoparticles make them attractive for use as nanoscale drug-delivery vehicles.

Keywords Temperature-responsive · pH-responsive · Hydrogel nanoparticles · Gold nanoparticles · Gold core–polymer shell · Drug delivery

Introduction

Organic shell/metal core hybrid nanocomposites, in which a layer of organic material surrounds or encapsulates a metal core, have received substantial attention with regard to their fabrication and potential applications in areas such as electronics (Klein et al. 1997), optics (Chen and Sommers 2001; Quaroni and Chumanov 1999; Teranishi and Miyake 1998), biotechnology (Haes and Van Duyne 2002; McFarland and Van Duyne 2003; Storhoff et al. 2000), and chemical catalysis (Bergbreiter et al. 1998; Jeong et al. 1997). Commonly, an organic layer made up of small molecules, DNA (Cao et al. 2001; Storhoff et al. 2000), or polymers (Miyazaki and Nakano 2000; Mossmer et al. 2000) is grafted "to" the surface of a metal core to combine their physical and chemical properties with that of the metal nanoparticles (MNPs). These hybrid nanocomposites often exhibit unique properties that are not possible from one component alone. Among the various shell/core structures, gold nanoparticles (AuNPs) whose surfaces have been selectively modified with functional organic molecules are of particular interest. This system is characterized by biocompatibility (Connor et al. 2005), the possibility

Electronic supplementary material The online version of this article (doi:10.1007/s11051-010-0180-3) contains supplementary material, which is available to authorized users.

H. H. Park · T. R. Lee (✉)
Department of Chemistry and The Texas Center for Superconductivity, University of Houston, Houston, TX 77204-5003, USA
e-mail: trlee@uh.edu

of chemically tailored functionalization via thiol chemistry (Daniel and Astruc 2004), and the localized surface plasmon resonance of the metal cores, which arises from light coupling to the collective oscillation of electrons at the metal surface (Kreibig and Vollmer 1995). The combination of the organic functional layer and the optical properties of the gold nanoparticles has led to the development of a variety of sensing applications. For example, Mirkin et al. reported that AuNPs functionalized with oligonuleotides acted as DNA and protein biosensors (Taton et al. 2001). Furthermore, Ipe et al. found that functionalization of AuNPs with 2,2′-bipyridine followed by complexation with lanthanide metal ions (e.g., europium and terbium) afforded selective sensors for biologically important cations (Ipe et al. 2006).

An alternative approach to the design of functionalized nanomaterials is based on the growth of preferred polymers "from" the surface of metal nanoparticles, leading to a polymer shell/metal core structure. To generate the polymer shell, initiators are immobilized on the surface of the nanoparticles, and then monomers are polymerized around the nanoparticles with the aid of the immobilized initiator. These shell/core particles often show enhanced physical and chemical properties compared to their isolated components, rendering them attractive for use in a broad range of applications. Furthermore, this strategy typically permits facile control over the thickness and the density of the polymer shell. In previous study utilizing this approach, AuNPs were encapsulated within poly(methyl methacrylate) by Ohno et al. (2002) and Mandal et al. (2002). Poly(butyl acrylate) has also been used to coat AuNPs (Nuss et al. 2001). More recently, Raula et al. reported the controlled radical polymerization of *N*-isopropylacrylamide on the surface of AuNPs (Raula et al. 2003).

Hydrogel polymers are macromolecular networks that swell in aqueous solution and absorb amounts of water several thousand times the equivalent of their dry weight (Hoffman 2002). With this swelling capacity, hydrogels can play key roles in a variety of applications, including drug delivery (Hoffman 2002; Kim et al. 1992), catalysis (Bergbreiter et al. 1998), and tissue engineering (Temenoff and Mikos 2000). Notably, hydrogels derived from *N*-isopropylacrylamide (NIPAM) have been thoroughly studied due to their unique temperature-responsive behavior, where they expand the structure at low temperature and collapse back the structure at high temperature. Several research groups have investigated the phase transition of NIPAM-based hydrogels in water (Debord and Lyon 2003; Gan and Lyon 2001; Nayak and Lyon 2004a, b; Wang et al. 2001; Wu and Zhou 1996, 1995). Furthermore, this temperature-responsive behavior of PNIPAM-based hydrogels has been incorporated into various types of applications, such as micro-lenses (Jones et al. 2003; Kim et al. 2005), ligand-functionalized shell/core microgels (Nayak and Lyon 2004a, b), and folate-conjugated hydrogels for the potential use of folate-targeted liposomes (Dube et al. 2002).

At low temperatures, poly(*N*-isopropylacrylamide) (PNIPAM) hydrogels are hydrophilic and swell in water via extensive hydrogen bonding. At elevated temperatures, however, the hydrogen bonds break, and the PNIPAM becomes hydrophobic through an entropically favored release of water, which leads to phase separation and collapse of the superstructure. The temperature at which the phase separation occurs is called the lower critical solution temperature (LCST), and PNIPAM exhibits an LCST at 32 °C (Prevot et al. 2006). Introducing acrylic acid (AA) monomer into the NIPAM polymer backbone raises the LCST of the copolymer from 32 °C to as high as 60 °C (Snowden et al. 1996) and makes the hydrogel responsive to changes in the pH of the solution. Under basic conditions, the PNIPAM-co-AA hydrogel superstructure is expanded; under acidic conditions, however, it collapses (Morris et al. 1997). Stimuli-responsive PNIPAM-based hydrogels thus undergo completely reversible swelling–deswelling volume changes in response to changes in both temperature and pH. Utilizing these properties, the hydrogels can release soluble materials held within the hydrogel matrix by collapsing their polymer network when the temperature of the polymer exceeds the LCST or when the pH decreases, making them attractive for use in controlled drug delivery (Nolan et al. 2004, Serpe et al. 2005, Kim and Lee 2006).

In the study reported here, we encapsulate AuNPs ($\sim$40 nm in diameter) within PNIPAM-co-AA copolymer hydrogels prepared using rationally designed surface-bound free radical initiators (see Fig. 1). Within the molecular structure shown, the thiol group at one end of the chain is used to anchor the initiator to the surface of the AuNP, and the PEG group at the other end is used

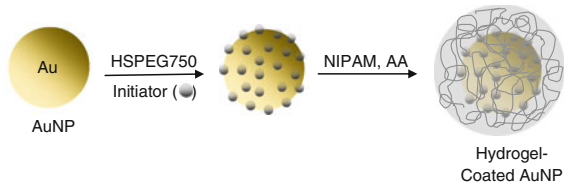

Fig. 1 Hydrogel growth on AuNPs using radical polymerization

initially to stabilize the AuNPs in solution and later to lend biocompatibility to the system (Harris et al. 2001). Upon mixing with AuNPs, the initiator molecules replace surface-associated citrate molecules, which were used to prepare and electrostatically stabilize the AuNPs. We then grow a PNIPAM-co-AA hydrogel shell via free radical polymerization initiated from the surface of AuNPs. Furthermore, we demonstrate that the hydrogel coatings undergo reversible swelling and deswelling upon systematic changes in temperature and pH.

Experimental section

Materials

The monomer *N*-isopropylacrylamide (NIPAM) was obtained from Acros (99.0%), recrystallized in hexane, and dried under vacuum before use. Acrylic acid (AA, Acros, 99.5%) and *N*,*N*′-methylenebisacrylamide (BIS, Acros, 96.0%) were used as received from the indicated suppliers. For the initiator synthesis, 4,4′-azobis(4-cyanovaleric acid) (Aldrich, 75+%), 1,6-hexanedithiol (Aldrich, 96.0%), poly(ethylene glycol) methyl ether (PEG750, Aldrich, Mn 750), *N*,*N*′-dicyclohexylcarbodiimide (DCC, Fluka, 99.0%), and 4-dimethylaminopyridine (DMAP, Acros, 99.0%) were used as received. Tetrahydrofuran (THF, Mallinckrodt Baker) was freshly distilled over a calcium hydride and collected immediately prior to use. Hexane, ethyl acetate, chloroform ($CHCl_3$), dichloromethane (CH_2Cl_2), and methanol (MeOH) were purchased from Mallinckrodt Baker and used without further purification. All water used in the reactions was purified to a resistance of 10 MΩ (Milli-Q Reagent Water System, Millipore Corporation) and filtered through a 0.2-μm filter to remove any particulate matter. In the preparation of gold nanoparticles, trisodium citrate (EM, 99.0%) and hydrogen tetrachloroaurate ($HAuCl_4$, Strem) were used without purification.

Preparation of AuNPs

AuNPs were prepared by the reduction of $HAuCl_4$ with trisodium citrate (Frens 1973). The size of AuNPs was evaluated by scanning electron microscopy, transmission electron microscopy, and dynamic light scattering. All glassware used in the preparation and storage of the AuNPs were treated with aqua regia, rinsed with water, and cleaned with piranha solution (7:3 concentrated H_2SO_4/30 wt% H_2O_2); *Caution: piranha solution reacts violently with organic materials and should be handled carefully!*

Synthesis of (R)-4-cyano-4-((E)-((R)-2-cyano-5-(6-mercaptohexylthio)-5-oxopentan-2-yl)diazenyl)-pentanoic acid (HS-NN-)

One end of 4,4′-azobis(4-cyanovaleric acid) was modified with 1,6-hexanedithiol using DCC/DMAP (see Fig. 2). Under argon, 5.00 g (17.9 mmol) of 4,4′-azobis(4-cyanovaleric acid) and 50 mg (0.41 mmol) of DMAP were combined with 2.68 g (17.9 mmol) of 1,6-hexanedithiol in 70 mL of anhydrous THF. The solution was cooled to 0 °C, and 3.68 g (17.9 mmol) of DCC in 50 mL THF was added drop-wise to the mixture with stirring. The reaction was allowed to proceed at 0 °C for 30 min, and then allowed to warm to room temperature and continue stirring for 24 h under argon. The urea precipitate was removed by filtration, and after the solvent was evaporated, the product was further purified by chromatography on silica gel using 6/4 hexane/ethyl acetate as the eluent to give the desired product as a clear oil (4.42 g; 10.7 mmol; 60% yield). ^{1}H NMR (in $CDCl_3$, δ in ppm): 2.89 (2H, t, $J = 6.9$ Hz), 2.49 (10H, m), 1.73 (3H, s), 1.68 (3H, s), 1.58 (4H, p, $J = 7.2$ Hz), 1.38 (4H, m). Using these data, we can exclude the possibility of macromolecule formation. Specifically, the inequivalence of the two methyl singlets at δ 1.73 and 1.68 in conjunction with their peak areas relative to that of the triplet for the thioester methylene at δ 2.89 is consistent with the monomeric structure proposed for HS-NN-.

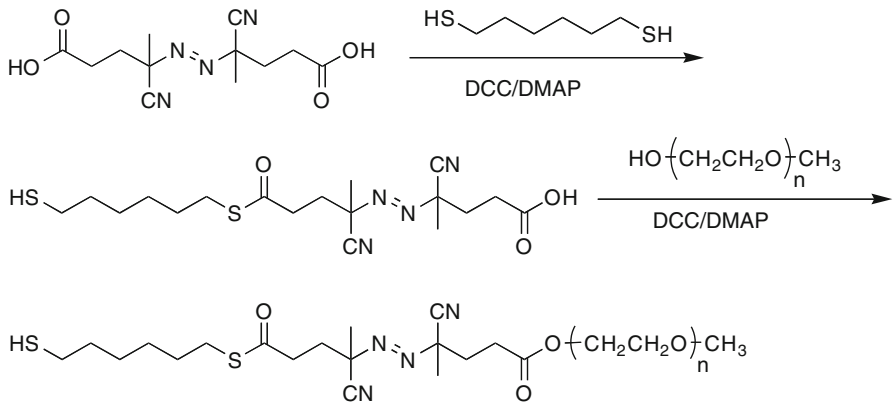

Fig. 2 Strategy used to prepare the initiator (HSPEG750), $n = \sim 16$

Synthesis of (E)-PEG750-4-cyano-4-((E)-((R)-2-cyano-5-(6-mercaptohexylthio)-5-oxopentan-2-yl)di-azenyl)pentanoic acid (HSPEG750)

The other end of HS-NN- was modified with PEG750 using conventional DCC/DMAP coupling (see Fig. 2). An aliquot (1.00 g; 2.43 mmol) of the pure thiolated acid was dissolved with 1.82 g (2.43 mmol) of poly(ethylene glycol) methyl ether (Mn 750, PEG750), and 30 mg (0.25 mmol) of DMAP in 50 mL of anhydrous THF under an atmosphere of argon. The solution was cooled to 0 °C, and 0.60 g (2.9 mmol) of DCC in 30 mL THF was added dropwise to the mixture with stirring. The mixture was allowed to stir at 0 °C for 30 min, and then allowed to warm to room temperature and stirred for 24 h under argon. The urea precipitate was removed by filtration, and the filtrate was poured into saturated sodium bicarbonate, extracted with CH_2Cl_2, and dried over magnesium sulfate. After the solvent was evaporated, the product was further purified by chromatography on silica gel using 95/5 $CHCl_3$/MeOH as the eluent to give the desired HSPEG750 as a clear oil (1.11 g; 0.97 mmol; 40% yield). ^{1}H NMR (in $CDCl_3$, δ in ppm): 4.26 (2H, t, $J = 3.3$ Hz), 3.75-3.53 (70H, m), 3.38 (3H, s), 2.89 (2H, t, $J = 6.9$ Hz), 2.49 (10H, m), 1.73 (3H, s), 1.68 (3H, s), 1.58 (4H, p, $J = 7.2$ Hz), 1.38 (4H, m).

Immobilization of initiators and polymerization of NIPAM-co-AA on the surface of AuNPs

An aliquot (10 mL) of the aqueous suspension of AuNPs described above (40 nm in diameter; $\sim 8 \times 10^{10}$ particles/mL) was mixed with a 1 mM solution of HSPEG750 in ethanol (3 mL) for 30 min, and this mixture was allowed to stand at room temperature for 24 h. The initiator-functionalized AuNPs were washed by centrifugation at 6,000 rpm with water twice and ethanol twice before use. The hydrogel-coated AuNPs were prepared by free radical polymerization in aqueous solution by the following procedure: initiator-functionalized AuNPs were dispersed in 60 mL water, and then 10 mL of NIPAM (0.01 M; 0.10 mmol), 1 mL of AA (0.01 M; 0.01 mmol), and 1 mL of BIS (0.01 M; 0.01 mmol) were added to the solution. The mixture was stirred and bubbled with argon for 1 h to remove oxygen, which can intercept radicals. To effect the polymerization, the solution was heated to 65 °C in an oil bath and stirred for 6 h under argon. The solution was then cooled to 20 °C. All particles were purified by dialysis (Spectra/Por Dialysis Membrane, MWCO 12–14,000, VWR) against daily changes of water for 1 week at 25 °C.

Characterization of nanoparticles

To characterize the bare AuNPs, initiator-functionalized AuNPs, and the hydrogel-coated AuNPs, we used X-ray photoelectron spectroscopy (XPS), scanning electron microscopy (SEM), transmission electron microscopy (TEM), dynamic light scattering (DLS), and ultraviolet–visible (UV–Vis) spectroscopy.

XPS spectra of the initiator-functionalized AuNPs were collected using a PHI 5700 X-ray photoelectron spectrometer equipped with a monochromatic Al Kα X-ray source ($h\nu = 1486.7$ eV) incident at 90 °C relative to the axis of a hemispherical energy analyzer.

An aqueous suspension of AuNPs (10 mL) was mixed with a 1 mM solution of HSPEG750 in ethanol (3 mL) for 30 min, and this mixture was allowed to stand at room temperature for 24 h. The initiator-functionalized AuNPs were washed by centrifugation as described in a preceding paragraph. The initiator-functionalized AuNPs were then deposited onto a silicon wafer, and the solvent was allowed to evaporate before analysis. XPS scans were conducted at high resolution with a pass energy of 23.5 eV, a photoelectron takeoff angle of 45°, and an analyzer spot diameter of 2 nm. The base pressure in the chamber during the measurements was 3×10^{-9} Torr, and the spectra were collected at room temperature. After collecting the data, the binding energies of the S and C peaks were referenced by setting the $Au_{4f7/2}$ binding energy to 84 eV.

Analysis by SEM was performed using a LEO Scanning Electron Microscope with 20 kV of accelerating voltage during the measurements. Bare AuNPs and hydrogel-coated AuNPs were deposited on silicon wafers and dried at room temperature to collect the images. SEM was used to examine the overall morphology of the bare AuNPs and hydrogel-coated AuNPs. Similarly, TEM images of the nanoparticles were collected using a JEM-2000 FX electron microscope (JEOL) operating at an electron voltage of 200 kV. The samples were prepared by placing small drops of the solution onto 300-mesh Holey carbon-coated copper grids and drying before analysis.

For the DLS measurements, an ALV-5000 Multiple Tau Digital Correlation instrument was used, operating at a light source wavelength of 514.5 nm and a fixed scattering angle of 90°. The diameter of the bare AuNPs was measured at room temperature. The hydrodynamic diameter of the hydrogel-coated AuNPs was measured as a function of temperature and pH in water. The samples were analyzed at dilute concentrations, and all of the data collected showed good Gaussian distribution curves.

The optical properties of the AuNPs and the hydrogel-coated AuNPs were monitored at room temperature using a Cary 50 Scan UV–Vis optical spectrometer (Varian) in conjunction with Cary Win UV software. UV–Vis spectra of the prepared nanoparticles were collected in solution over a wavelength range 400–900 nm in a quartz cuvette having a 1 cm optical path length.

Results and discussion

Immobilization of initiators on the surface of AuNPs

The initiator HSPEG750 was immobilized on the surface of the AuNPs via ligand exchange. The citrate molecules, which were initially surrounding and stabilizing the AuNPs via electrical repulsion (Mirkin 2000), can be displaced by the –SH group of the initiators due to the formation of a strong covalent bond between the sulfur headgroup and the surface of gold (Lin et al. 1990). Since chemical bonding influences the electron distribution in the atoms of interest, the Au–S bond can be verified by using XPS to measure the atomic binding energy of sulfur. In particular, the S_{2p} region of the XPS spectra can provide evidence for bond formation between the sulfur atom and the gold substrate, although spin-orbital coupling can inhibit an accurate analysis as it gives rise to a doublet with a split of 1.2 eV (Castner et al 1996; Laibinis et al. 1991). In analysis by XPS, the binding energy of the $S_{2p3/2}$ peak for thiols bound to gold is 162 eV; in contrast, the $S_{2p3/2}$ peak for unbound thiols appears at 164 eV (Castner et al. 1996), which is also the characteristic energy of the $S_{2p3/2}$ peak for thioester (Wenzler et al. 1997). Based on these precedents, we used XPS to evaluate the immobilization of the initiator on the surface of the AuNP prior to polymerization. In our analyses, we calibrated the binding energies by setting the $Au_{4f7/2}$ peak at 84 eV.

Figure 3a shows the XPS spectra of the $S_{2p3/2}$ region for the initiator-functionalized AuNPs. The presence of a covalent bond between the initiators and the AuNPs was verified with the appearance of a relatively weak $S_{2p3/2}$ peak at 162 eV. The appearance of a stronger $S_{2p3/2}$ peak at 164 eV arises from either incomplete adsorbate binding of the initiator molecules or the sulfur atom in the thioester tailgroup or a combination of both. It is difficult to distinguish these possibilities given the uncertainties involved in estimating the relative attenuation of sulfur-derived photoelectrons, which vary with the myriad of possible positions around the AuNPs. Nevertheless, we know that the sulfur atoms of the thiol headgroups are predominantly located at the gold surface, and the sulfur atoms of the thioester groups are predominantly located at the periphery of the

composite particle. In contrast to homogeneously distributed materials, the analysis of layered structures XPS is complicated by attenuation effects that tend to underestimate the elements buried deeper relative to those on the periphery (Lu et al. 2000; Wenzler et al. 1997). As such, the smaller intensity of the $S_{2p3/2}$ peak at 162 eV relative to that of the $S_{2p3/2}$ peak at 164 eV in Fig. 3a can be rationalized in the context of a model in which all of the initiator molecules are covalently bound to the surface of the AuNPs.

To probe the viability of this model, we used the initiator molecules to form self-assembled monolayers (SAMs) on the surface of an evaporated gold film and analyzed the SAMs by XPS. To form the SAMs, the gold substrate was immersed in a 1 mM ethanolic solution of the initiator and allowed to equilibrate for 48 h. The slide was exhaustively rinsed with toluene and ethanol to remove any unbound initiator molecules, and then dried under a rigorous stream of nitrogen before analysis by XPS (Park et al. 2005). As shown in Fig. 3b, similar spectra were obtained in the S_{2p} region of the SAM system even though the films were thoroughly washed. These observations support the conclusion above that the initiator molecules are covalently bound to the surface of the AuNPs.

Polymerization of NIPAM-co-AA on the surface of AuNPs

To encapsulate the AuNPs within a NIPAM-co-AA polymer shell, a mixture of initiator-functionalized AuNPs, NIPAM, AA, and BIS (cross-linker) was stirred in degassed water for 6 h at 65 °C under argon. The immobilized initiator was thermally activated to induce radical polymerization on the surface of the 40 nm AuNP cores, generating a ~60 nm thick PNIPAM-co-AA hydrogel shell. The resulting hydrogel-coated AuNPs were characterized by SEM and TEM as shown in Fig. 4. The SEM images in Fig. 4a show that almost all of the AuNPs were encapsulated with complete PNIPAM-co-AA shells. Furthermore, the TEM images in Fig. 4b show a thick polymer halo surrounding the AuNP cores, providing evidence that PNIPAM-co-AA hydrogel-coated AuNPs were successfully synthesized. Importantly, the strategy reported here circumvents the formation of any core-less hydrogel particles, which has plagued some of our previous study in this area (Kim and Lee 2004).

Thermal and pH responsiveness of NIPAM-co-AA hydrogel-coated AuNPs

We used dynamic light scattering (DLS) in water to monitor the behavior of the bare AuNP cores and hydrogel-coated AuNPs in response to changes in temperature and pH. Figure 5a shows the hydrodynamic diameter of the nanoparticles as a function of temperature. Bare AuNPs exhibited no temperature-dependent behavior; however, hydrogel-coated AuNPs showed a reversible change of ~40 nm in diameter. Starting above the LCST, the hydrodynamic diameter of the shell/core nanoparticle decreased from 160 to 120 nm as the temperature was increased. Collapse of the hydrogel at the LCST is known to arise from the loss of hydrogen bonding between water molecules and hydrophilic sites in the hydrogel polymer (Shibayama et al. 1996). At higher temperatures, the hydrogen bonds break, and there is an entropically favored release of water, leading to a

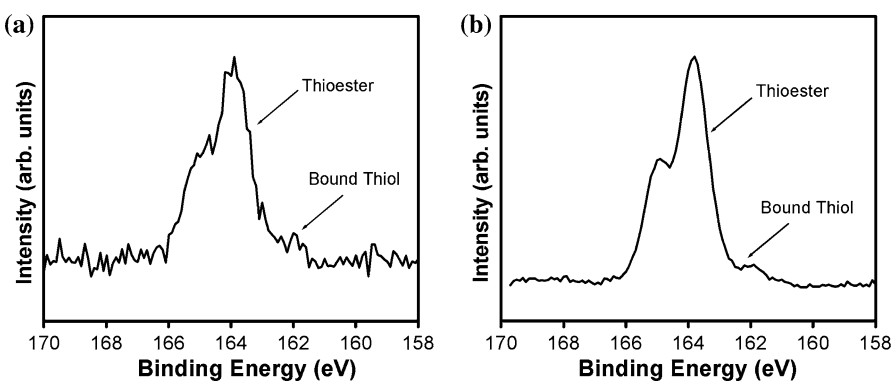

Fig. 3 XPS spectra of the S_{2p} region for (**a**) initiator-functionalized AuNPs and (**b**) SAMs derived from the initiator on an evaporated-functionalized flat gold surface

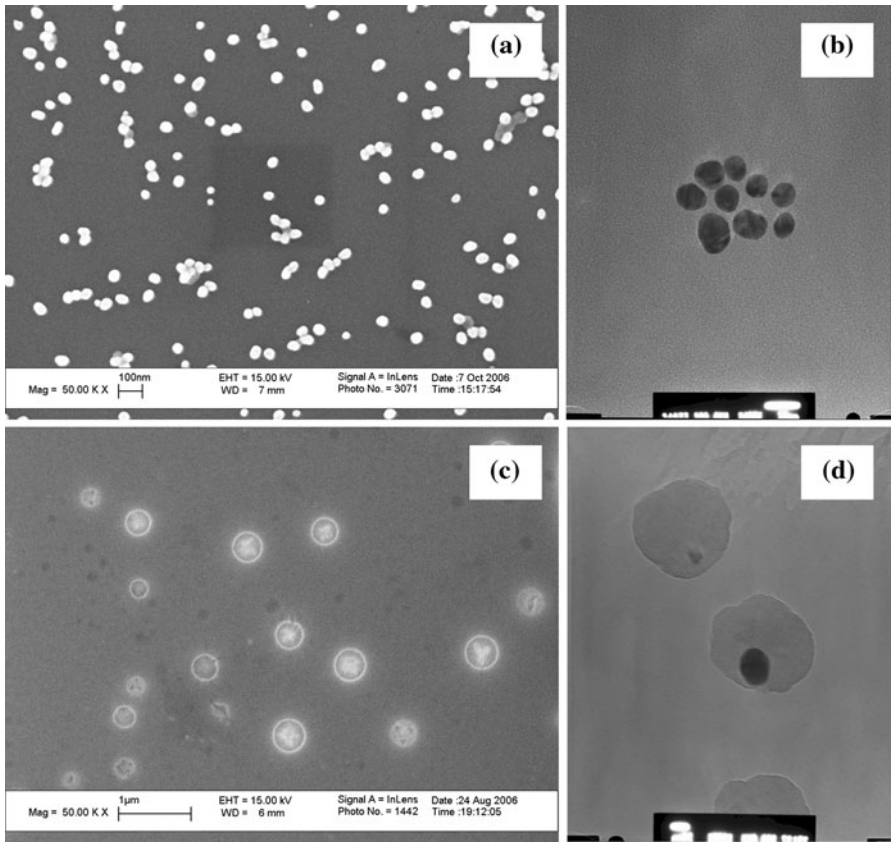

Fig. 4 Bare AuNPs imaged by (**a**) SEM and (**b**) TEM. Hydrogel-coated AuNPs imaged by (**c**) SEM and (**d**) TEM, *scale bar* 20 nm

collapse of the swollen structure. Specifically, the plot in Fig. 5a can be interpreted to indicate that the LCST of the PNIPAM-co-AA polymer (5 wt% AA) is 34 °C, which is consistent with that reported previously (Morris et al. 1997).

Figure 5b shows the hydrodynamic diameter of the composite nanoparticles as a function of solution pH. While bare AuNPs showed no change in diameter with varying pH, the hydrogel-coated AuNPs exhibited a reversible change of ~70 nm in diameter. The pH range for the swelling–collapsing transition of the shell/core nanoparticles occurs between pH 4 and 6, which is consistent with the known pKa value of 4.25 for AA (Morris et al. 1997). Under basic conditions, the hydrogel coating is expanded due to internal electrostatic repulsion between the anionic carboxylate groups (Morris et al. 1997). Under acidic conditions, however, the coating shrinks due to neutralization of the carboxylic acid groups and the corresponding loss of electrostatic repulsion.

Optical properties of NIPAM-co-AA hydrogel-coated AuNPs

We characterized the optical properties of bare AuNP cores, HSPEG750-modified AuNPs, and hydrogel-coated AuNPs by UV–Vis spectroscopy. According to Mie theory, the surface plasmon absorption band of AuNPs occurs at 520–530 nm and can shift depending on the size or shape of the particles and the dielectric constant of the surrounding medium (Mayya et al. 1997; Mulvaney 1996). Figure 6 presents the UV–Visible spectra of the nanoparticles. The bare AuNPs and HSPEG750-modified AuNPs exhibit a maximum absorption band, λ_{max}, at ~530 nm, which is consistent with the formation of spherical AuNPs (Rivas et al. 2001). The hydrogel-coated AuNPs exhibited a λ_{max} at slightly longer wavelength (~537 nm). This small red shift is most probably related to a change in the local dielectric constant around the AuNPs as a consequence of the PNIPAM-co-AA encapsulation (Eck et al. 2001),

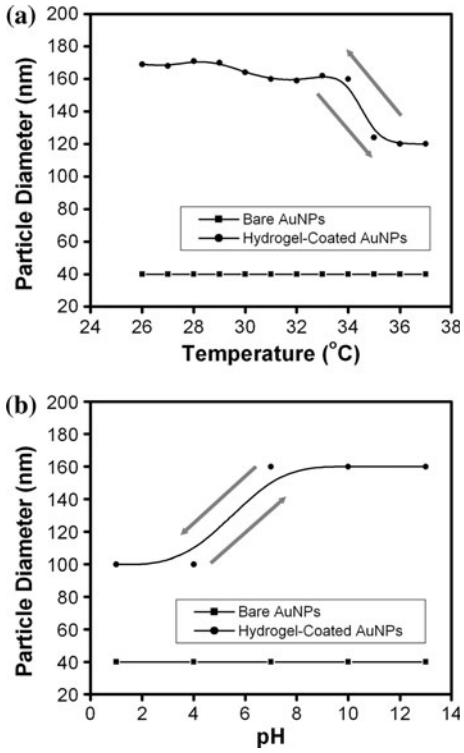

Fig. 5 The hydrodynamic diameter of bare AuNP cores and hydrogel-coated AuNPs as a function of (**a**) temperature and (**b**) pH

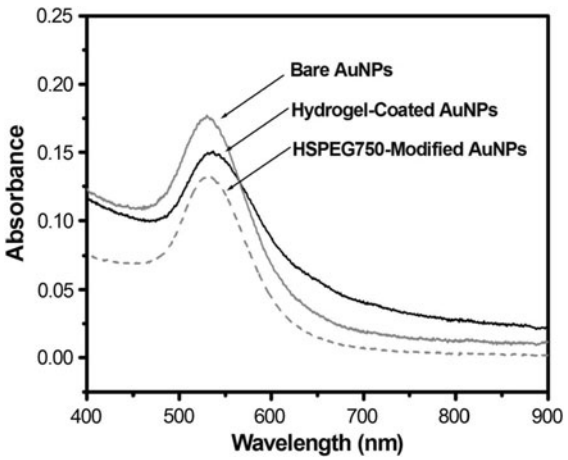

Fig. 6 UV–Vis spectra of bare AuNP cores, HSPEG750-modified AuNPs, and hydrogel-coated AuNPs

and thus supports the formation of the shell/core structure.

We are developing these types of composite nanoparticles for use in photothermally modulated drug delivery (Kim and Lee 2004, 2006). As light is absorbed by hydrogel-coated AuNPs, the gold cores become hot (Kim and Lee 2004, 2006, 2008). When the temperature in the vicinity of the AuNPs exceeds the LCST, the NIPAM-based hydrogel will collapse and release any drug molecules pre-loaded within the hydrogel network. Furthermore, the periphery of the PNIPAM-co-AA shell/gold core can be modified with targeting agents to direct the nanoscale vehicles to desired sites, thus enhancing the efficiency and lowering the toxicity of any embedded molecules. Studies of drug loading inside the hydrogel naoparticle network and modification of the hydrogel periphery with targeting molecules are currently underway, as are complementary studies using nanoshell cores, which can be activated by near-IR wavelengths for in vivo applications (Kim and Lee 2008).

Conclusions

Stimuli-responsive hydrogel-coated AuNPs were formed using a rationally designed surface-bound initiator. The diameter of the gold cores was ~40 nm, and the thickness of the PNIPAM-co-AA hydrogel coatings was ~60 nm, as judged by SEM and TEM. Notably, the nanoparticle synthesis strategy reported here efficiently circumvents the formation of any core-less hydrogel particles. The reversible thermal and pH responsiveness of the hydrogel-coated AuNPs was demonstrated using DLS, where the diameter of the hydrogel-coated AuNPs decreased with increasing temperature and decreasing pH. These results support our ongoing efforts to employ these types of composite particles as discrete nanoscale drug-delivery vehicles.

Acknowledgments We are grateful for generous financial support from the Robert A. Welch Foundation (Grant No. E-1320) and the Texas Center for Superconductivity.

References

Bergbreiter DE, Case BL, Liu YS, Caraway JW (1998) Poly (*N*-isopropylacrylamide) soluble polymer supports in catalysis and synthesis. Macromolecules 31:6053–6062

Cao YW, Jin R, Mirkin CA (2001) DNA-modified core-shell Ag/Au nanoparticles. J Am Chem Soc 123:7961–7962

Castner DG, Hinds K, Grainger DW (1996) X-ray photoelectron spectroscopy sulfur 2p study of organic thiol and

disulfide binding interactions with gold surfaces. Langmuir 12:5083–5086
Chen S, Sommers JM (2001) Alkanethiolate-protected copper nanoparticles: spectroscopy, electrochemistry, and solid-state morphological evolution. J Phys Chem B 105:8816–8820
Connor EE, Mwamuka J, Gole A, Murphy CJ, Wyatt MD (2005) Gold nanoparticles are taken up by human cells but do not cause acute cytotoxicity. Small 1:325–327
Daniel M-C, Astruc D (2004) Gold nanoparticles: assembly, supramolecular chemistry, quantum-size-related properties, and applications toward biology, catalysis, and nanotechnology. Chem Rev 104:293–346
Debord JD, Lyon LA (2003) Synthesis and characterization of pH-responsive copolymer microgels with tunable volume phase transition temperatures. Langmuir 19:7662–7664
Dube D, Francis M, Leroux J-C, Winnik FM (2002) Preparation and tumor cell uptake of poly(*N*-isopropylacrylamide) folate conjugates. Bioconjugate Chem 13:685–692
Eck D, Helm CA, Wagner NJ, Vaynberg KA (2001) Plasmon resonance measurements of the adsorption and adsorption kinetics of a biopolymer onto gold nanocolloids. Langmuir 17:957–960
Frens G (1973) Controlled nucleation for the regulation of the particle size in monodisperse gold suspensions. Nature Phys Sci 241:20–22
Gan D, Lyon LA (2001) Tunable swelling kinetics in core-shell hydrogel nanoparticles. J Am Chem Soc 123:7511–7517
Haes AJ, Van Duyne RP (2002) A nanoscale optical biosensor: sensitivity and selectivity of an approach based on the localized surface plasmon resonance spectroscopy of triangular silver nanoparticles. J Am Chem Soc 124:10596–10604
Harris JM, Martin NE, Modi M (2001) Pegylation: a novel process for modifying pharmacokinetics. Clin Pharmacokinet 40:539–551
Hoffman AS (2002) Hydrogels for biomedical applications. Adv Drug Delivery Rev 54:3–12
Ipe BI, Yoosaf K, Thomas KG (2006) Functionalized gold nanoparticles as phosphorescent nanomaterials and sensors. J Am Chem Soc 128:1907–1913
Jeong B, Bae YH, Lee DS, Kim SW (1997) Biodegradable block copolymers as injectable drug-delivery systems. Nature 388:860–862
Jones CD, Serpe MJ, Schroeder L, Lyon LA (2003) Microlens formation in microgel/gold colloid composite materials via photothermal patterning. J Am Chem Soc 125:5292–5293
Kim J-H, Lee TR (2004) Thermo- and pH-responsive hydrogel-coated gold nanoparticles. Chem Mater 16:3647–3651
Kim J-H, Lee TR (2006) Discrete thermally responsive hydrogel-coated gold nanoparticles for use as drug-delivery vehicles. Drug Dev Res 67:61–69
Kim J-H, Lee TR (2008) Thermo-responsive hydrogel-coated gold nanoshells for in vivo drug delivery. J Biomed Pharma Eng 2:29–35
Kim SW, Bae YH, Okano T (1992) Hydrogels: swelling, drug loading, and release. Pharm Res 9:283–290
Kim J, Nayak S, Lyon LA (2005) Bioresponsive hydrogel microlenses. J Am Chem Soc 127:9588–9592
Klein DL, Roth R, Lim AKL, Alivisatos AP, McEuen PL (1997) A single-electron transistor made from a cadmium selenide nanocrystal. Nature 389:699–701
Kreibig U, Vollmer M (1995) Optical properties of metal clusters. Springer, New York
Laibinis PE, Whitesides GM, Allara DL, Tao YT, Parikh AN, Nuzzo RG (1991) Comparison of the structures and wetting properties of self-assembled monolayers of normal-alkanethiols on the coinage metal-surfaces, Cu, Ag, Au. J Am Chem Soc 113:7152–7167
Lin MY, Lindsay HM, Weitz DA, Ball RC, Klein R, Meakin P (1990) Universal reaction-limited colloidal aggregation. Phys Rev A 41:2005–2020
Lu HB, Campbell CT, Castner DG (2000) Attachment of functionalized poly(ethylene glycol) films to gold surfaces. Langmuir 16:1711–1718
Mandal TK, Fleming MS, Walt DR (2002) Preparation of polymer coated gold nanoparticles by surface-confined living radical polymerization at ambient temperature. Nano Lett 2:3–7
Mayya KS, Patil V, Sastry M (1997) On the stability of carboxylic acid derivatized gold colloidal particles: the role of colloidal solution pH studied by optical absorption spectroscopy. Langmuir 13:3944–3947
McFarland AD, Van Duyne RP (2003) Single silver nanoparticles as real-time optical sensors with zeptomole sensitivity. Nano Lett 3:1057–1062
Mirkin CA (2000) Programming the assembly of two- and three-dimensional architectures with DNA and nanoscale inorganic building blocks. Inorg Chem 39:2258–2272
Miyazaki A, Nakano Y (2000) Morphology of platinum nanoparticles protected by poly(*N*-isopropylacrylamide). Langmuir 16:7109–7111
Morris GE, Vincent B, Snowden MJ (1997) Adsorption of lead ions onto *N*-isopropylacrylamide and acrylic acid copolymer microgels. J Colloid Interface Sci 190: 198–205
Mossmer S, Spatz JP, Moller M, Aberle T, Schmidt J, Burchard W (2000) Solution behavior of poly(styrene)-block-poly(2-vinylpyridine) micelles containing gold nanoparticles. Macromolecules 33:4791–4798
Mulvaney P (1996) Surface plasmon spectroscopy of nanosized metal particles. Langmuir 12:788–800
Nayak S, Lyon LA (2004a) Ligand-functionalized core/shell microgels with permselective shells. Angew Chem Int Ed 43:6706–6709
Nayak S, Lyon LA (2004b) Photoinduced phase transitions in poly(*N*-isopropylacrylamide) microgels. Chem Mater 16: 2623–2627
Nolan CM, Serpe MJ, Lyon LA (2004) Thermally modulated insulin release from microgel thin films. Biomacromolecules 5:1940–1946
Nuss S, Bottcher H, Wurm H, Hallensleben ML (2001) Gold nanoparticles with covalently attached polymer chains. Angew Chem Inter Ed 40:4016–4018
Ohno K, Koh K, Tsujii Y, Fukuda T (2002) Synthesis of gold nanoparticles coated with well-defined, high-density polymer brushes by surface-initiated living radical polymerization. Macromolecules 35:8989–8993
Park J-S, Vo AN, Barriet D, Shon Y-S, Lee TR (2005) Systematic control of the packing density of self-assembled monolayers using bidentate and tridentate chelating alkanethiols. Langmuir 21:2902–2911

Prevot M, Dejugnat C, Mohwald H, Sukhorukov GB (2006) Behavior of temperature-sensitive PNIPAM confined in polyelectrolyte capsules. ChemPhysChem 7:2497–2502

Quaroni L, Chumanov G (1999) Preparation of polymer-coated functionalized silver nanoparticles. J Am Chem Soc 121: 10642–10643

Raula J, Shan J, Nuopponen M, Niskanen A, Jiang H, Kauppinen EI, Tenhu H (2003) Synthesis of gold nanoparticles grafted with a thermoresponsive polymer by surface-induced reversible-addition-fragmentation chain-transfer polymerization. Langmuir 19:3499–3504

Rivas L, Sanchez-Cortes S, Garcia-Ramos JV, Morcillo G (2001) Growth of silver colloidal particles obtained by citrate reduction to increase the Raman enhancement Factor. Langmuir 17:574–577

Serpe MJ, Yarmey KA, Nolan CM, Lyon LA (2005) Doxorubicin uptake and release from microgel thin films. Biomacromolecules 6:408–413

Shibayama M, Mizutani S, Nomura S (1996) Thermal properties of copolymer gels containing *N*-isopropylacrylamide. Macromolecules 29:2019–2024

Snowden MJ, Chowdhry BZ, Vincent B, Morris GE (1996) Colloidal copolymer microgels of *N*-isopropylacrylamide and acrylic acid: pH, ionic strength and temperature effects. J Chem Soc Faraday Trans 92:5013

Storhoff JJ, Lazarides AA, Mucic R, Mirkin C, Letsinger R, Schatz GC (2000) What controls the optical properties of DNA-linked gold nanoparticle assemblies? J Am Chem Soc 122:4640–4650

Taton TA, Lu G, Mirkin CA (2001) Two-color labeling of oligonucleotide arrays via size-selective scattering of nanoparticle probes. J Am Chem Soc 123:5164–5165

Temenoff JS, Mikos AG (2000) Injectable biodegradable materials for orthopedic tissue engineering. Biomaterials 21:2405–2412

Teranishi T, Miyake M (1998) Size control of palladium nanoparticles and their crystal structures. Chem Mater 10:594–600

Wang J, Gan D, Lyon LA, El-Sayed MA (2001) Temperature-jump investigations of the kinetics of hydrogel nanoparticle volume phase transitions. J Am Chem Soc 123: 11284–11289

Wenzler LA, Moyes GL, Raikar GN, Hansen RL, Harris JM, Beebe TP, Wood LL, Saavedra SS (1997) Measurements of single-molecule bond-rupture forces between self-assembled monolayers of organosilanes with the atomic force microscope. Langmuir 13:3761–3768

Wu C, Zhou S (1995) Laser light scattering study of the phase transition of poly(*N*-isopropylacrylamide) in water. 1. Single chain. Macromolecules 28:8381–8387

Wu C, Zhou S (1996) Internal motions of both poly(*N*-isopropylacrylamide) linear chains and spherical microgel particles in water. Macromolecules 29:1574–1578